

Chapter 2

Artifacts Correction in MRI Images

2.1 Existing Methods

1. Ultra-echo time imaging (UTE).
2. Sweep imaging with Fourier transform.
3. Water- and fat-suppressed proton projection MRI.
4. ZTE imaging without including the excitation profile.

2.1.1 Disadvantages of Ultra-echo Time Imaging (UTE)

1. Compared to UTE, ZTE traverses k-space faster, resulting in higher signal-to-noise ratio (SNR) and reduced blurring due to less T2 decay within the data acquisition window.
2. The image distortion artifact associated with ramp sampling in UTE imaging is avoided.

2.1.2 Disadvantages of Sweep Imaging with Fourier Transform

1. Sweep imaging with Fourier transform uses the Fourier transforms.
2. It is a time-consuming process.

2.1.3 Disadvantages of Water- and Fat-suppressed Proton Projection MRI

1. Acquisition of additional radial projections with lower gradient strength is required.

2.1.4 Disadvantages of ZTE Imaging Without Excitation Profile

1. Problems can arise in ZTE due to the imaging gradient being on during hard pulse excitation.
2. Inverse problem arises.
3. ZTE imaging does not include the excitation profile.

2.2 Implemented Method

In this work, we model the ZTE sequence signal to include the excitation profile effect, and formulate a correction algorithm as a solution to an inverse problem. In order to eliminate the zero crossings in the sinc excitation profile and to condition the inverse problem, we propose to modulate the hard RF pulse with quadratic phase, which produces a flatter excitation profile. The RF pulse excitation profile can be measured using a simple pulse sequence. Without loss of generality, we apply our method to one variant of ZTE imaging sequences, namely PETRA. By combining phase-modulated RF excitation and iteratively solving the inverse problem, results from simulations, phantom, and in vivo studies demonstrate the effectiveness of our method for correcting image artifacts caused by inhomogeneous excitation, even when the extent of the imaged object exceeds the main lobe of the sinc function (Fig. 2.1).

2.3 Process Diagram

In proposed system, firstly, the uncorrected ZTE image which is obtained from MRI Scanner is converted to system matrix by applying the spatial transformation and then performed the non-uniform FFT to obtain the radial trajectories of the original image. The NUFFT operator maps the image to k-space radial spokes, with one spoke for each radial trajectory, and another spoke for each Cartesian point. Each spoke is separated by zero-padding with a factor of two, multiplied with the excitation profile, and finally restoring the original vector length. Dirichlet interpolation in the Cartesian portion is performed for mapping the Cartesian

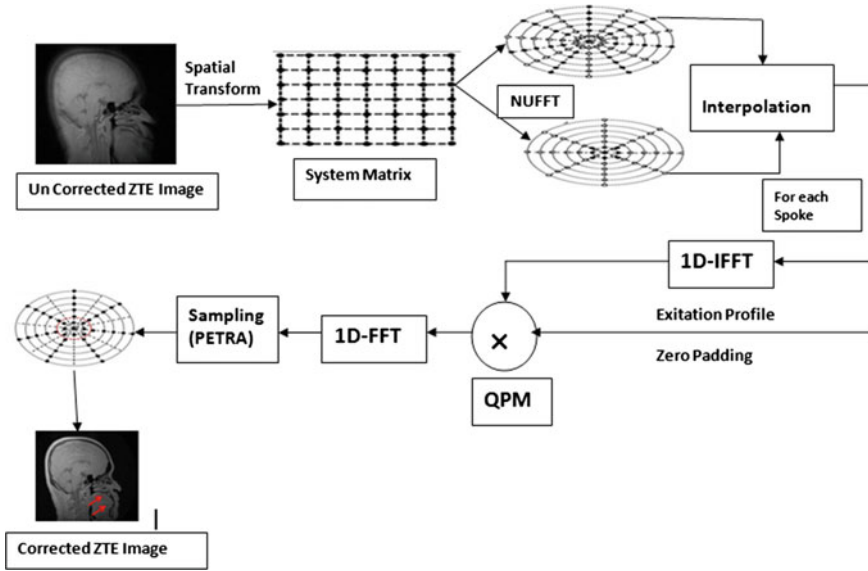


Fig. 2.1 Proposed process diagram

coordinates of the single points to coincide with those in the radial spokes. Finally, the corrected ZTE image is obtained by perform sampling (PETRA).

System matrix composed of three sequential operators: The NUFFT operator, the excitation profile modulation operator, and the sampling operator. The solid dots represent the acquired samples in-space, and the hollow circles denote the locations which are interpolated by NUFFT but not acquired by the sequence.

The proposed algorithm has three main parts:

- (A) Model as an inverse problem
- (B) Quadratic phase-modulated hard RF pulse
- (C) Excitation profile measurement

2.4 Model as an Inverse Problem

The fundamental problem in medical imaging is to reconstruct an image of something inside the human body from minimally invasive and nondestructive measurements. The measurements are related to the quantities of interest by a mathematical model, which usually describes how the unknown system would produce the measured values. The basic inverse problem is to determine the system from sufficiently many measurements. The analysis of the inverse problem is made by the following parameters.

1. Uniqueness: Decide which measurements Y suffice, in principle, to determine the value X .
2. Reconstruction: From an exact inversion algorithm B to find exact data Y . This sometimes involves characterizing the range of A that the set of possible measurements.
3. Practical implementation: A stable, accurate approximation to B that can be applied to a finite, noisy set of measurements.

The corrected image with hard RF pulse excitation profile fits within the main lobe of the sinc-shaped excitation profile, if not then the amplified noise causes inversion of the ill-conditioned matrix rooted from the zero crossings of the sinc function which corrupts the resulting image. Generally, the residual artifacts are appeared in outside of the spherical region defined by the main lobe of the sinc-shaped profile. This is because the null points in the excitation profile cause the system matrix to be singular and make the inverse problem. The best case scenario is represented by MRI. The inverse problem is simply inversion of the Fourier transform measurements.

In order to eliminate image artifacts, the effect of the non-uniform excitation profile needs to be considered in image reconstruction.

The discretization yields to

$$S(k_j) = \sum_{i=1}^N m(r_i) p(G_j, r_i) e^{-i2\pi(k_j, r_i)} + \varepsilon_j \quad j = 1, 2, \dots, M$$

where

N is the number of pixels of the reconstructed image, and

M is the number of space samples.

The image reconstruction algorithm was implemented in MATLAB with NUFFT algorithm as a mex function written in C. The corrected image with hard RF pulse excitation profile fits within the main lobe of the sinc-shaped excitation profile. If these conditions are not met, the amplified noise causes inversion of the ill-conditioned matrix rooted from the zero crossings of the sinc function would corrupt the resulting image. Here, the residual artifact outside the spherical region is defined by the main lobe of the sinc-shaped profile. This is because the null points in the excitation profile cause the system matrix to be singular and make the inverse problem ill-conditioned.

2.5 NUFFT Operator

NUFFT operator maps the (Cartesian) image onto space (full) radial spokes, with one spoke for each radial trajectory, and additionally one spoke for each Cartesian point. The operator acts on each projection separately by zero-padding (by a factor

of two), 1D IFFT, multiplication with the excitation profile, 1D FFT, and finally restoration of the original vector length. The sampling operator, denoted, masks out the fraction of the radial signal that was not acquired (recall that less than half of each radial spoke is acquired) and performs Dirichlet interpolation in the Cartesian portion (since the coordinates of the single points may not coincide with those in the radial spokes). Application of the operator is the most time-consuming process, requiring computations. The adjoint operator is the reverse process of the above steps. The image reconstruction algorithm was implemented in MATLAB (Mathworks, Natick, MA, USA) with NUFFT algorithm as a mex function written in C.

A good way to think of the NUDFT is in terms of interpolation. In general, NUDFT is essentially the DFT without limitations to equally spaced frequency nodes and useful for applications in which samples must be taken at irregular intervals in frequency, time, or both (NNDFT), allows for more “selectively concentrated” frequency (or time) information.

Fast implementation: `NUFFT::NUDFT::FFT:DFT`

NUDFT—Non-uniformly spaced or non-equispaced discrete Fourier Transform. The DFT and FFT are limited to obtaining frequency information at regular intervals in the frequency domain when given samples were taken at regular intervals in the time/space domain. In many applications, the data will be collected on a non-uniform grid, or it is desirable to have the frequency information for non-uniformly spaced points in the frequency domain. In these cases, we can use a generalization of the DFT known as the non-uniform DFT. The non-uniform DFT will assume equispacing in time/space but will allow spacing in the frequency domain to be variable. A further generalization of the NUDFT is the NNDFT, which does not assume equispacing in either domain. The mathematics is a little trickier, but essentially the problem is exactly the same. The fast version of the NUDFT is the NUFFT, as you might expect.

Interpolation can be thought of as two sequential processes. Firstly, FFT was taken to get frequency information at uniformly spaced nodes, and secondly results are used to interpolate into desired nodes. Approximation interpolation only produces approximation of values at desired nodes. Quality of approximation depends on node spacing and nature of function.

In 1D, frequency information for certain frequencies is required. First, find a linear combination of 1-periodic shifted window functions to approximate the NUDFT. To simplify the development, we can just look at how the NUFFT is done in one dimension. Our goal is to find weights for a linear combination of 1-periodic shifted window functions that we can use to approximate the NUDFT well. We want to select the window function and the window function weights in such a way that we can get our approximated signal as close as possible to the NUDFT. In the equation on the slide, little $n = \text{sigma} * N$. This is just meant to indicate that we have oversampled the function by a factor sigma, but it is important because it will be used in our approximations.

Above method is essentially used as method of frequency interpolation. Started with a standard window function, can extend to 1-periodic version. The window

functions essentially serve as methods of frequency interpolation. By coming up with a general expression for the transform of our data, we can evaluate it at specific frequencies, as we said before. The shifted window functions, then, are linearly combined to give us a continuous function we can evaluate at certain points. If we start with some window function ϕ , we can extend it to a 1-periodic version and then express it as a Fourier Series with coefficients as on the slide.

While the NUDFT computes the Fourier coefficients in one fell swoop, it is instructive to think of it as two processes that occur in serial. First, the input data is used to perform a standard FFT and get Fourier coefficients on a regularly spaced grid. Using these, the frequency representation of the signal can be interpolated to find the values at the desired frequency nodes. Because this process uses interpolation, it only produces an approximation of the coefficients at these nodes. The quality of that approximation will depend on the specific behavior of the function being transformed and the spacing of the nodes

2.5.1 Features of NUFFT

1. It is computationally fast.
2. Full calculation of A does not required.
3. It is not a real representation of the transform because here approximations in both time/space and frequency.
4. It uses the window operations and FFT techniques.

The NUFFT is similar to the FFT in the sense that it is a fast algorithm for the NUDFT transform, but there is a key difference to it—it does not give a perfect representation of the NUDFT. Just as with the DFT, it is impractical and computationally expensive to construct the entire NUDFT matrix.

2.5.2 Non-uniform FFT Algorithm

By making use of simple FFT algorithms, the system matrix cannot be generated, as when the data is sampled by using the non-uniform grid with spiral sampling trajectories projections. In order to perform for the non-uniform grid, a number of FFT algorithms came into existence to get frequency information at uniformly spaced nodes in which the results are used to interpolate into desired nodes. Moreover, several algorithms have been proposed; the easiest and simple NUFFT algorithm is as follows:

1. For $k \in I_N$, compute $W_k = g_k / \text{INlck}(c)$
2. For $q \in I_N$, compute by use of the d-variate FFT $W_q = \sum_{k \in I_N} W_k e^{-2\pi i k(n^{-1}\theta q)}$

3. For $j = 0, \dots, M - 1$, Compute $g(f_j) = \sum_{q \in I_{N,m(x_j)}} W_q(f_j - n^{-1}\Theta q)$

Using these approximations, if we are given the number of Fourier coefficients M , the vector N of data points in each dimension, the frequency locations, and the data values themselves, we can compute the NUFFT.

First, we determine the time/space weights by dividing them by the known Fourier coefficients for our chosen window function and by the cardinality of the set I_N .

We only do this for k in I_N ; we set the time/space weights for k in I_N but not N to 0.

Then, for each vector in I_N , we determine the frequency weight by performing a d -variate FFT on the weights w_k that we computed.

Finally, we can write our approximation as a linear sum of the shifted window functions and evaluate this at the frequency nodes f_j to get our Fourier coefficients at the desired locations.

2.6 Quadratic Phase-Modulated RF Pulse Excitation

A quadratic phase-modulated rectangular (chirped) pulse was designed for excitation instead. As shown in both simulations and experiments, the corrected image with hard RF pulse excitation shows residual artifact outside the spherical region defined by the main lobe of the sinc-shaped profile. This is because the null points in the excitation profile cause the system matrix to be singular and make the inverse problem ill-conditioned.

In order to eliminate the zero crossings of the rectangular pulse excitation profile, a quadratic phase is modulated to the RF pulse waveform

$$B_1(t) = \begin{cases} b_1, e^{-i2\pi k(\frac{t}{T})^2} & \text{if } |t| \leq \frac{T}{2} \\ 0, & \text{elsewhere} \end{cases}$$

which controls the amount of quadratic phase applied to the RF pulse. In all of the following applications, K is set to 1. The corresponding excitation profile can be computed by numerical Bloch equation simulation. The quadratic phase-modulated pulse has a flatter excitation profile than does a simple hard pulse. More importantly, no zero-crossing point occurs in the profile even when the pulse duration is four times that of the dwell time.

When a quadratic phase modulation is applied to the RF pulse, the excitation profile becomes flatter and lacks a null point, as shown in the Bloch equation simulation results. This improved excitation profile can be understood as a type of regularization to physically reduce the condition number of the inverse problem. The sinc-shaped hard pulse excitation profile is pure real. As a way to remove the null point, an imaginary part is added into the profile to make it complex. Hence, the magnitude of the profile is no longer singular. The improvement in the

reconstructed images is evident. The amount of phase modulation applied to the RF pulse constitutes a trade-off between the flip angle and the minimum value of the absolute magnetization profile within the field of view. Application of too much phase yields low flip angle for a given peak B_1 amplitude and pulse duration.

On the other hand, inadequate quadratic phase causes the magnetization profile to approach a sinc profile, and the noise will be amplified due to a close-to-singular system matrix. Here, we chose a relatively small amount of quadratic phase in order to achieve minimal flip angle loss while maintaining a relatively flat excitation profile.

2.6.1 *Hard RF Phase Modulation*

The quadratic-phase pulses can be appreciated by matching up to linear-phase pulses. Mostly, the magnetization in the selected bands is turn around simultaneously with a linear-phase pulse. The short main lobe is considered, as its width is inversely proportional to the bandwidth.

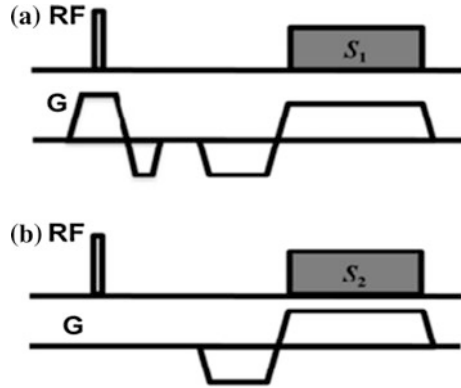
$$W \propto 1/B$$

If quadratic phase modulation is applied to the RF pulse, the excitation profile becomes flatter and lacks a null point. The hard pulse sinc-shaped excitation profile is pure real; to remove the null point, an imaginary part is added into the profile to make it complex. So, the magnitude of the profile is no longer singular. The improvement in the reconstructed images is evident. The total of phase modulation is applied to the RF pulse where it constitutes a trade-off between the flip angle and the minimum value of the absolute profile. To eliminate the zero crossings of the rectangular pulse excitation profile, a quadratic phase is modulated to the RF pulse waveform.

2.7 **Excitation Profile Measurement**

A pulse sequence was proposed to measure the excitation profile, which can be inserted as a prescan into the ZTE sequence. Firstly, the profile was obtained by measuring the actual pulse shape with an oscilloscope and then by taking the Fourier transform of the pulse shape. In this method one does not require additional hardware and is an optional component into the ZTE pulse sequence. The spectral profile measured by the new sequence shows good agreement with that obtained from the Bloch equation simulation. Therefore, we conclude that the profile from the numerical simulation is sufficiently accurate as an input for the correction algorithm.

Fig. 2.2 Signals acquired by the first and second acquisitions



In order to confirm that we indeed achieve the theoretical excitation profile, we propose a simple pulse sequence for its measurement, which can be inserted as a prescan into the ZTE sequence. The improved excitation profile can be understood as a type of regularization to physically reduce the condition number of the inverse problem. The sinc-shaped hard pulse excitation profile is pure real. As a way to remove the null point in excitation profile, an imaginary part is added into the profile to make it complex (Fig. 2.2).

Suppose the signals acquired by the first and second acquisitions are S_1 and S_2 , respectively. The excitation profile $p(f)$ is calculated as

$$P = \frac{FT - 1(S_1)}{FT - 1(S_2)}$$

A sketch of this pulse sequence is shown in Fig. 2.4a, b. Suppose the signals acquired by the first and second acquisitions are S_1 and S_2 , respectively, we calculated the excitation profile.

2.8 Pointwise Encoding Time Reduction with Radial Acquisition (PETRA)

Some of the parameters limit the minimum encoding time for each k-space point. They are scanner's gradient performance, pulse length, and hardware switching times. One of the features in PETRA pointwise encoding time reduction with radial acquisition is the radial half-projections is present in outer k-space whereas center portion is filled with Cartesian trajectory.

It is three-dimensional method which offers shorter encoding times over the whole k-space which enables higher resolution for tissue with very short T_2 . It has very low demands on gradient switching times and is not disturbed by gradient imperfections such as eddy currents and time delays which lead to a problem for

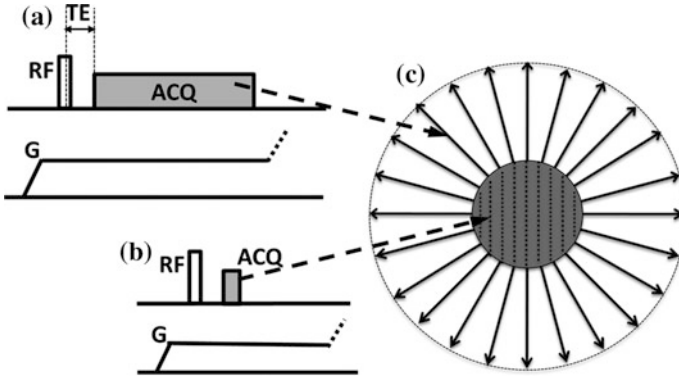


Fig. 2.3 Pulse sequence diagram of PETRA, consisting of **a** radial acquisition, **b** Cartesian portion, and **c** corresponding space trajectory

UTE imaging. PETRA in ZTE gives good signal-to-noise ratio (SNR) for tissue with short T2 and good image quality overall (Fig. 2.3).

The features of radial projection imaging are combines with single point imaging using this hybrid sequence. Hardware changes are not required. Three-dimensional isotropic resolution images can be acquired within three minutes of 1 mm by implementing this method. We obtain the comparison between the ultrashort echo time and the pointwise encoding time reduction with radial acquisition can be observed by simulation and phantom measurements. As it requires T2 tissue with less than 1 ms, it is the advantage of pointwise encoding time reduction with radial acquisition. Some of the limitations of this method can be seen by using the Contrast-to-noise ratio performance and SNR. The phantom and vivo studies of knee, ankle, head, and wrist examples give the sequences of more feasibility. PETRA is helpful in routine clinical applications using the ultrashort echo time sequences and also in fast imaging with ultrashort echo time.

The outer k-space in pointwise encoding time reduction with radial acquisition is filled with radial half-projections whereas the center is measured single point on a Cartesian trajectory. The crossbreed sequence combines the features of single point imaging with radial projection imaging. No hardware changes are required.

2.9 Iterative Partial K-Space Reconstruction

The methods of the previous section perform the reconstruction in one pass. Problems arises from the interaction between phase correction and the conjugate synthesis method, as was described above. Another approach is to estimate the missing k-space data by iteratively applying phase correction and conjugate synthesis. In the image domain, the image phase is constrained to be that of the low-resolution estimate. In the frequency domain, the k-space data is constrained to

match the acquired data when available. Iterating produces an estimate that approximately satisfies both sets of constraints. There are several variations on this idea, depending on how the constraints are applied, and how the iteration is performed.

Iterative reconstruction is a relatively new concept for the calculation of medical images, which is based on formulating the reconstruction process mathematically as an inverse problem and solving it with a numerical optimization method. Driven by recent success for dose reduction in CT, iterative reconstruction is currently receiving strong interest also in the MRI community. The first part of the iterative reconstruction scheme talk will give a step-by-step introduction and tells how to use it for the magnetic resonance imaging.

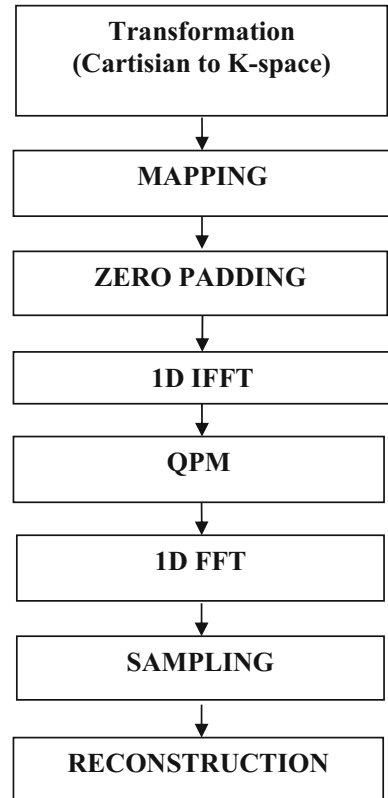
The second part will present four applications to illustrate that the concept can be exploited either for significantly reducing the scan time or for improving the image quality relative to a conventional reconstruction. The above advantages were taken from two main components of the sampled data: Firstly, the incorporation of prior knowledge about the solution and, second, the use of an extended modeling of the MRI signal.

Quadratic phase modulation with iterative reconstruction is applied to the RF pulse, the excitation profile becomes flatter and lacks a null point, as shown in the Bloch equation simulation results. It is a new concept for the calculation of medical images, based on formulating the reconstruction process mathematically as an inverse problem and solving it with a numerical optimization method. Iterative reconstruction is currently receiving strong interest in the MRI community. Iterating produces an estimate that approximately satisfies both sets of constraints. There are several variations on this idea, depending on how the constraints are applied, and how the iteration is performed.

2.10 Processing of Project

- Step 1: Transforming the Cartesian form of image into k-space by applying the NUFFT.
- Step 2: NUFFT operator maps the (Cartesian) image to k-space (full) radial spokes, with one spoke for each radial trajectory and additionally one spoke for each Cartesian point.
- Step 3: The P operator acts on each projection separately by zero-padding (by a factor of two), 1D IFFT, and multiplication with the excitation profile.
- Step 4: By applying 1D FFT, original vector length is restored.
- Step 5: The sampling operator masks out the fraction of the radial signal that was not acquired (recall that less than half of each radial spoke is acquired) and performs Dirichlet interpolation in the Cartesian portion.
- Step 6: Applying of the NUFFT operator is the most time-consuming process, requiring $O(N \log N)$ computations. The adjoint operator is the reverse process of the above steps.

Fig. 2.4 Flow diagram of implemented method



Step 7: The image reconstruction algorithm was implemented in MATLAB (Mathworks, Natick, MA, USA) with NUFFT algorithm as a mex function written in C (Fig. 2.4).

2.11 Flow Diagram

Simulation Results

The uncorrected ZTE image from MRI scanner is processed through RF phase modulation; the corrected ZTE image is obtained for different iterations. The maximum artifacts are reduced by processing the uncorrected image for number of iterations.

Figure 2.5 shows the single uncorrected coronal view of Brain input image is processed by QPM to correct the uncorrected ZTE image and enhanced reconstructed image for 30 iterations.

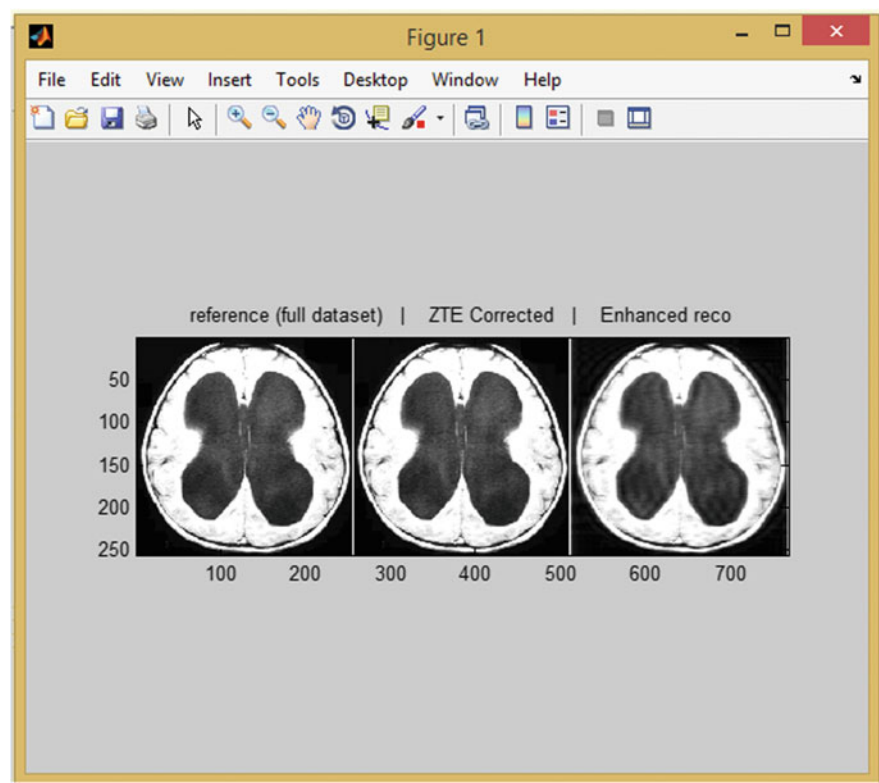


Fig. 2.5 ZTE corrected and enhanced image of 30 iterations

Figure 2.6 shows the amount of artifacts correction for 30 iterations by comparing the initial image with enhanced reconstructed image.

Figure 2.7 shows the uncorrected coronal view of Brain input image is processed by QPM to correct the uncorrected ZTE image and enhanced reconstructed image for 100 iterations.

Figure 2.8 shows the amount of artifacts correction for 100 iterations by comparing the initial image with enhanced reconstructed image (Table 2.1).

As the number of iterations increased, the artifacts gets minimized. From the above table, the iterations increase from 30 to 100; the mean square error is decreased from 2.7 to 2.2; and the peak SNR is increased from 13.66 to 14.62 which shows the artifacts gets reduced.

Figure 2.9 shows the one uncorrected coronal view of Brain and one uncorrected sagittal view input image are processed by QPM to correct the uncorrected ZTE image and enhanced reconstructed image for 30 iterations.

Figure 2.10 shows the amount of artifacts correction for 30 iterations by comparing the initial image with enhanced reconstructed image.

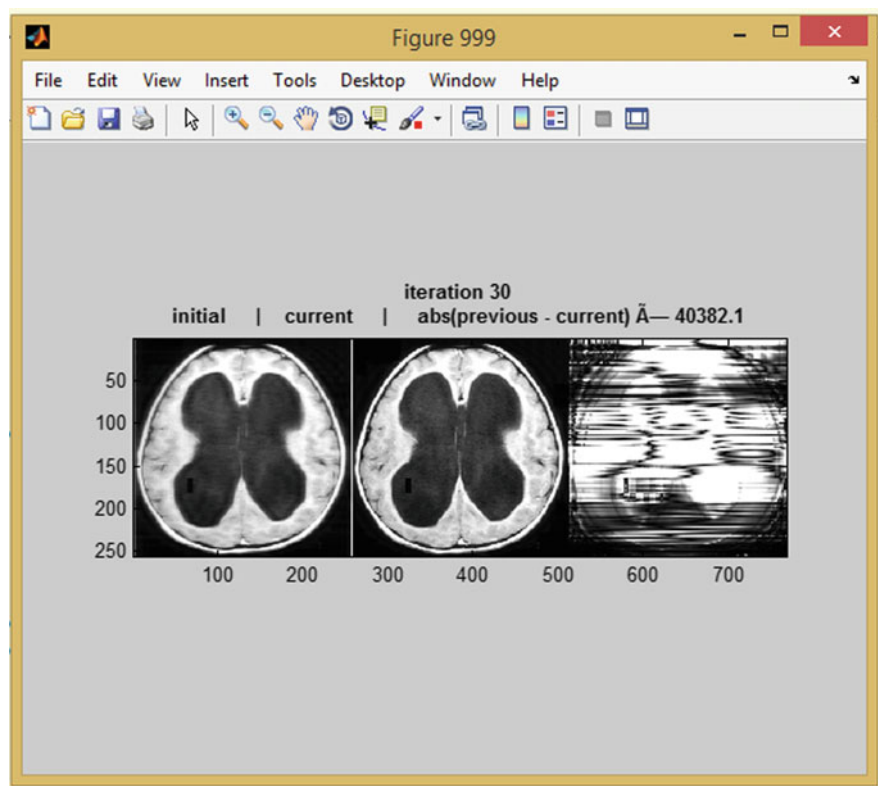


Fig. 2.6 Artifacts correction for 30 iterations

Figure 2.11 shows the one uncorrected coronal view of Brain and one uncorrected sagittal view input image are processed by QPM to correct the uncorrected ZTE image and enhanced reconstructed image for 100 iterations.

Figure 2.12 shows the amount of artifacts correction for 100 iterations by comparing the initial image with enhanced reconstructed image (Table 2.2).

As the number of iterations increased, the artifacts get minimized. From the above table, the iterations increase from 30 to 100; the mean square error is decreased from 2.7 to 2.2; and the peak SNR is increased from 13.66 to 14.62 which shows the artifacts gets reduced.

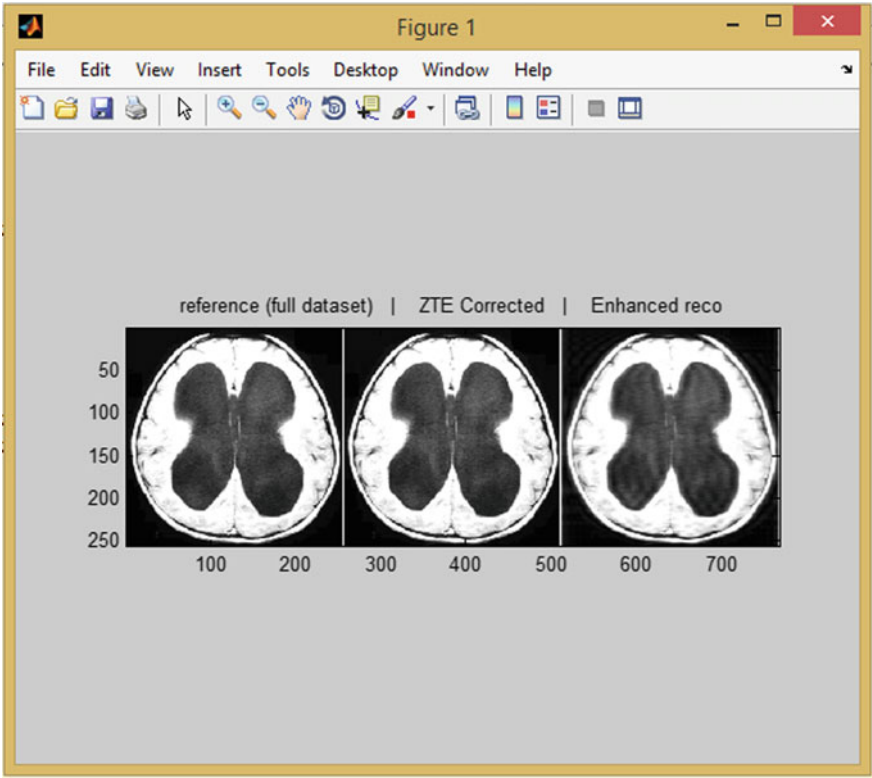


Fig. 2.7 ZTE corrected and enhanced image of 100 iterations

Discussions

MRI scanners use magnetic fields and radio waves to form images of the body. The MRI is widely used in hospitals for staging of disease and medical diagnosis of diseases and for follow-up without exposure to radiation. Nowadays, magnetic resonance imaging (MRI) is a unique clinical and research imaging technology that enables users to visualize different anatomical, metabolic, and physiological properties of the human body. These work on the majority species in tendons, ligaments, menisci, periosteum, cortical bone, and other related tissues.

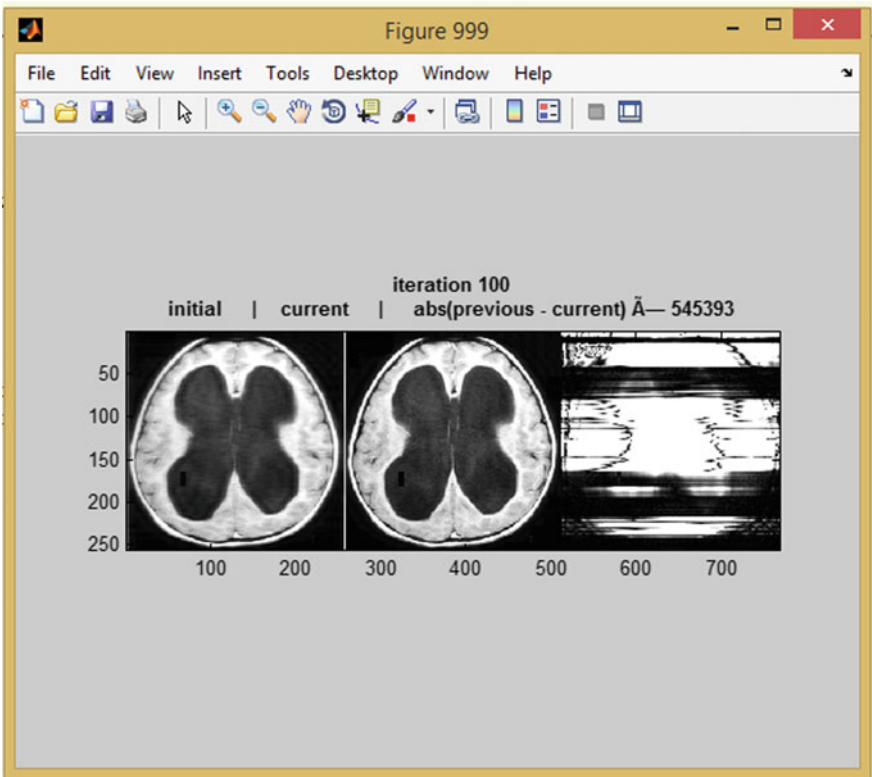


Fig. 2.8 Artifacts correction of single image for 100 iterations

Table 2.1 Statistical analysis values

S. No.	Parameter	Statistical value for 30 iterations	Statistical value for 100 iterations
1	Mean square error	2.7977e+003	2.2395e+003
2	Peak signal-to-noise ratio	13.6628	14.6293
3	Normalized cross-correlation	0.9448	0.9813
4	Average difference	−6.4536	−4.4867
5	Structural content	0.9215	0.9655
6	Maximum difference	232	196

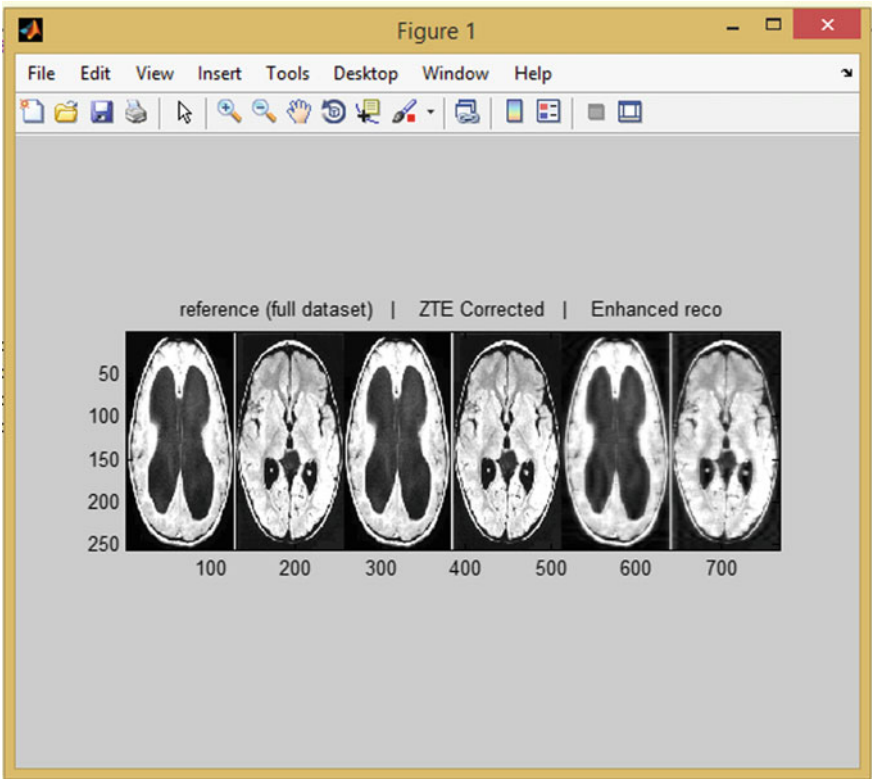


Fig. 2.9 ZTE corrected and enhanced of two images of 30 iterations

In this method, a new technique is implemented for reducing the artifacts in MRI images. In this work, the sequence of signals is used which include the flatter excitation profile which is obtained by modulate the hard RF pulse with quadratic phase and efficient algorithms. In this work, the iterative reconstruction is implemented for reduction of artifacts and also performed the simulation results. If the iterations is increased, the artifacts are reduced.

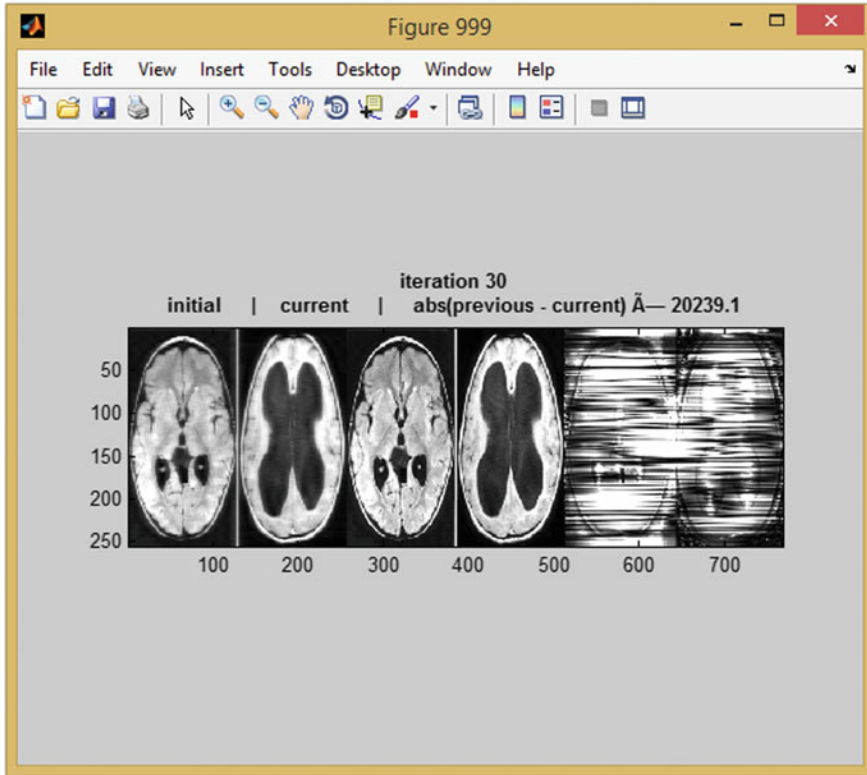


Fig. 2.10 Artifacts correction of two images for 30 iterations

Advantages

1. The ZTE sequence signal includes the excitation profile effect.
2. The inverse problem is reduced.
3. It produces the flatter excitation profile.
4. We can apply our method with PETRA sequence.

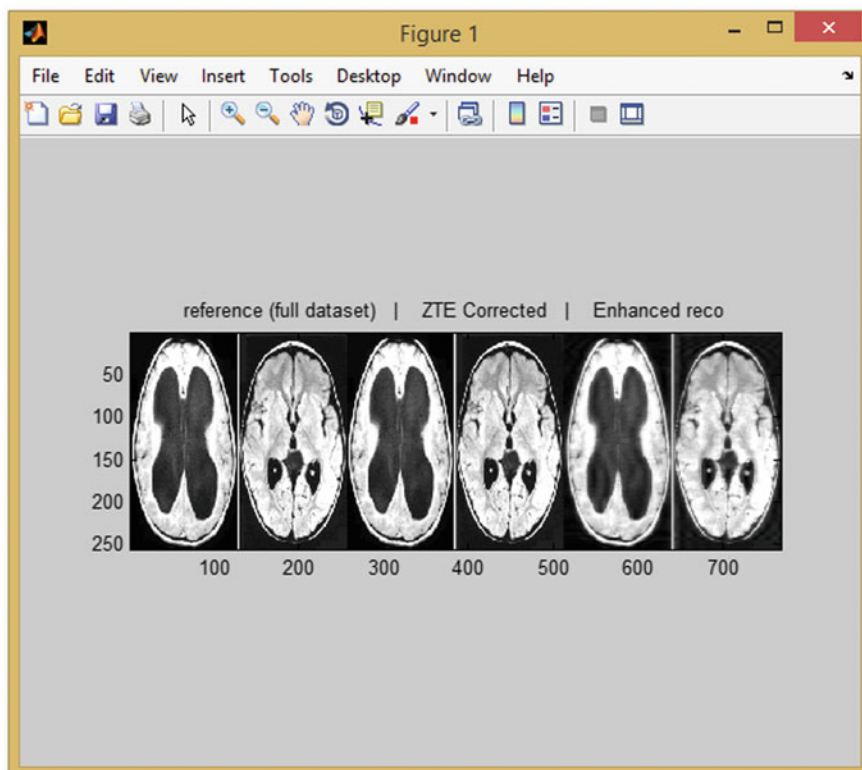


Fig. 2.11 ZTE corrected and enhanced of two images of 100 iterations

Disadvantages

1. This algorithm works under the condition that the object is inside the main lobe of the sinc-shaped excitation profile of the rectangular pulse.
2. In ZTE imaging, the gradients are present during hard pulse excitation.

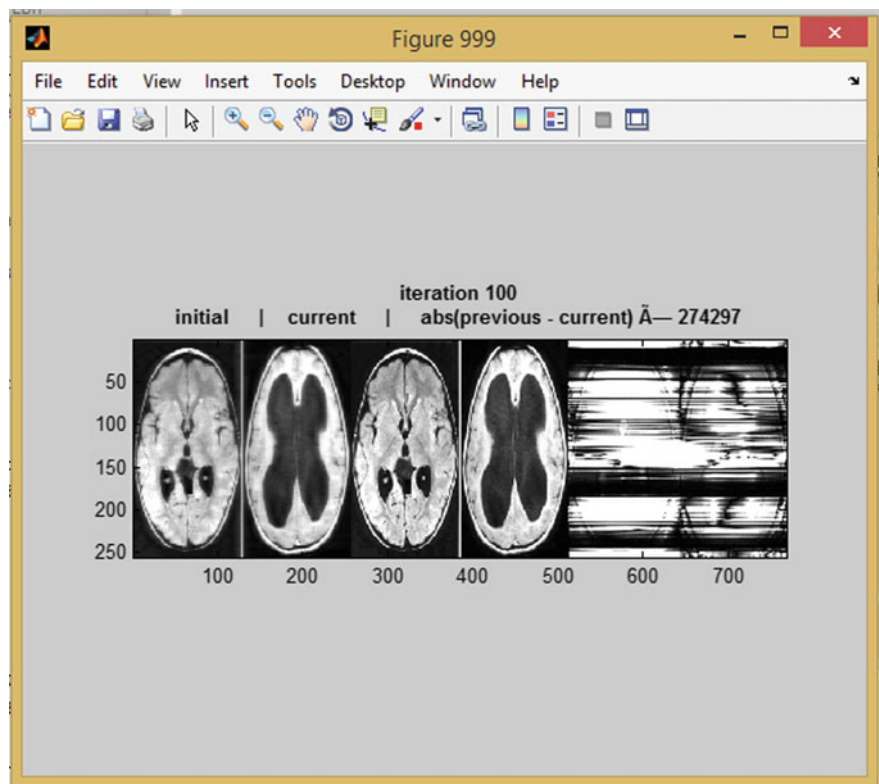


Fig. 2.12 Artifacts correction of two images for 100 iterations

Table 2.2 Statistical analysis

S. No.	Parameter	Statistical value for 30 iterations	Statistical value for 100 iterations
1	Mean square error	3.2515e+003	1.7224e+003
2	Peak signal-to-noise ratio	13.0100	15.7694
3	MN normalized cross-correlation	0.9270	0.9871
4	Average difference	−5.3624	−2.4307
5	Structural content	0.9436	0.9926
6	Maximum difference	227	147

Future Scope

The proposed method may be contributed toward establishing ZTE MRI as a routine 3D pulse sequence for imaging protons and other nuclei with quasi solid-state behavior on clinical scanners.

Computational Methods in Molecular Imaging
Technologies

Gunjan, V.K.; Shaik, F.; Venkatesh, C.; Amarnath, M.
2017, XV, 75 p. 52 illus., 17 illus. in color., Softcover
ISBN: 978-981-10-4635-3